N-156,886

NASA-TT-20117 19870018211

NASA TECHNICAL TRANSLATION NASA TT-20117

STUDY OF A VARIABLE SWEEP WING IN SUB OR TRANSONIC FLOW

F. Manie, C. Rehbach, V. Schmitt

LIBRARY COPY

SEP 28 1987

LANGLEY RESEARCH CENTER
LIBRARY, NASA
HAMPTON, VIRGINIA

Translation of "Etude d'une aile a fleche variable en ecoulement sub ou transonique", in: International Council of the Aeronautical Sciences, Congress, 11th, Lisbon, Portugal, September 10-16, 1978, Proceedings, Volume 2, 81A14391.

NATIONAL AERONAUTICS AND SPACE ADMINISTRATION
WASHINGTON D.C. 20546 SEPTEMBER 1987

STANDARD TITLE PAGE

1. Report No.	2. Government Accession No.	3. Recipient's Catalog No.
NASA TT-20177		

4. Title and Subtitle	5. Report Date
STUDY OF A VARIABLE SWEEPWWING IN SUB OR TRANSONIC FLOW	September 1987
	6. Performing Organization Code

7. Author(s)	8. Performing Organization Report No.
F. Manie, C. Rehback, V. Schmitt	
	10. Work Unit No.

9. Performing Organization Name and Address	11. Contract or Grant No.
Leo Kanner Associates Redwood City, CA 94063	NASw-4005
	13. Type of Report and Period Covered
	Translation
12. Sponsoring Agency Name and Address	14. Sponsoring Agency Code
National Aeronautics and Space Administration Washington, D.C. 20546	

15. Supplementary Notes

Translation of "Etude d'une aile a fleche variable in ecoulement sub or transsonique" in: International Council of The Aeronautical Sciences Congress, 11th, Lisbon, Portugal, September 10-16, 1978, Proceedings, Volume 2, 81A14391.

16. Abstract

Detailed experiments were performed on models of a variable sweep wing emphasizing in particular flow separation and appearance of vortex structures at low speeds and the formation of shock waves at transonic speeds. The results of these tests wre compared with those of calculations made by available processes such as a panel method for unseparated flows and un unsteady method based on a volume discretization of the vortex vector for separated flows. Transonic flows were calculated using different relaxation methods; one based on the perturbation theory, the other on the full potential equation.

For original see
A81-14391

17. Key Words [Selected by Author(s)]	18. Distribution Statement
	Unclassified-Unlimited

19. Security Classif. (of this report)	20. Security Classif. (of this page)	21. No. of pages	22.
Unclassified	Unclassified		

STUDY OF A SWEEP WING IN A SUB OR TRANSONIC FLOW

F. Manie, C. Rehbach, V. Schmitt

1 - INTRODUCTION /1*

A variable sweep wing was selected at ONERA to serve as a support for the study of three-dimensional flow up to transonic speeds, the guideline being to obtain as accurate and detailed experimental data as possible to meet the following two-fold objective:

-to improve the understanding of certain complex phenomena such as the mechanisms of a three-dimensional separation at low speeds, with or without organized separation, and of interference problems such as shock wave/boundary layer or apex vortex/shock wave problems;

-furthermore, to apply three-dimensional computer methods available and to determine their range of validity.

The purpose of the report is to show under this two-fold aspect a few meaningful results. In this context our intent is therefore not to describe the computer methods used in detail, nor to describe their expected developments, but rather to succintly show their capabilities and their current limitations from the user's standpoint.

2 - TEST MEANS AND METHODS

2.1 - Characteristics of Variable Sweep Wing Models

As shown in the diagram of figure 1 the AFV-D variable sweep wing is a rectangular wing with an ONERA "D" symmetrical profile (e/c = 0.105) with a "peaky" nature, the sweep of which is obtained by rotation about an axis.

*Numbers in the margin indicate pagination in the original text.

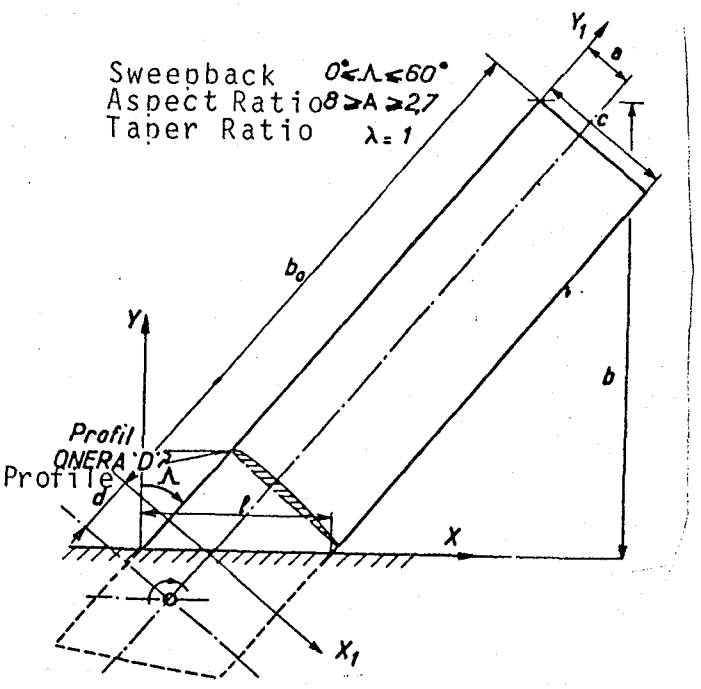

Fig. 1 - AFV-D Variable Sweep Wing

This design involves a large variation in the aspect ratio as a function of the sweep which may reach $\Lambda = 60°$. Two models of this wing were made. The first one (MS), used for studies at low speeds has a chord c = 0.3 m. The second (MT), designed for transonic experiments, is smaller (c = 0.2m).

The main geometrical features of these models are shown in figure 1. When the wing is placed in a sweep, a few differences pertain to the aspect ratio between the two models. The origin of this lies in the respective positions of the rotation axis about which the wing pivots. The coordinates of the ONERA 'D' profile are shown in Table 2.

Table 1 - AFV-D Geometry /2

MS: Subsonic Model
MT: Transonic Model

a=0,150 m d=0,060 m
a=0,075 m d=0,070 m

Λ°	Root Chord l(m) 1	2	Half Span b(m) 1	2	Aspect Ratio A 1	2	Wetted Area $S_o(m^2)$ 1	2
0	0,300*	0,200	1,200	0,800	8,00	8,00	0,3600	0,1600
30	0,346	0,231	1,107	0,721	6,86	6,71	0,3573	0,1550
40	0,392	0,261	1,002	0,645	5,66	5,49	0,3546	0,1515
50	0,467	0,311	0,865	0,547	4,28	4,09	0,3500	0,1463
60	0,600	0,400	0,700	0,430	2,87	2,69	0,3420	0,1373

*Commas in tabulated material are equivalent to decimal points.

Table 2 - Dimensions of "D" Profile

x_1/c	z_1/c	x_1/c	z_1/c
.000000	.000000	.072500	-.035193
.000050	-.001342	.077500	-.035912
.000200	-.002685	.082500	-.036604
.000500	-.004245	.087500	-.037269
.001000	-.006002	.092500	-.037908
.001700	-.007820	.105000	-.039405
.002600	-.009658	.120000	-.041028
.003700	-.011494	.135000	-.042486
.005000	-.013310	.155000	-.044213
.006500	-.015091	.195000	-.047057
.008300	-.016913	.235000	-.049242
.010300	-.018639	.275000	-.050853
.012500	-.020259	.315000	-.051902
.015000	-.021821	.355000	-.052369
.017500	-.023144	.395000	-.052230
.020000	-.024277	.435000	-.051476
.022500	-.025254	.475000	-.050123
.025000	-.026106	.520000	-.047942
.027500	-.026857	.580000	-.044120
.030000	-.027528	.640000	-.039509
.032500	-.028136	.690000	-.035239
.035000	-.028696	.730000	-.031601
.037500	-.029221	.770000	-.027763
.040000	-.029719	.810000	-.023691
.042500	-.030198	.850000	-.019335
.045000	-.030663	.890000	-.014658
.047500	-.031119	.930000	-.009698
.052500	-.032003	.970000	-.004621
.057500	-.032850	.990000	-.002090
.062500	-.033663	1.000000	-.000780
.067500	-.034444		

Table 3 - Position of Pressure Tap Sections

MS MODEL:

Sections		1	2	3	4	5	6
Y_1/b_o	A	0,05	0,10	0,20	0,30	0,40	0,50
	B	0,075	0,15	0,25	0,35	0,45	0,55
Sections		7	8	9	10	11	
Y_1/b_o	A	0,60	0,70	0,80	0,90	0,975	
	B	0,65	0,75	0,85	0,95	0,99	

MT MODEL:

Sections	1	2	3	4	5	6
Y_1/b_o	0,30	0,45	0,60	0,75	0,85	0,95

The measuring equipment for the two models has a very large number of static pressure taps. Thus the MS model has 341 pressure taps distributed twice into 11 sections and the MT model 246 pressure taps distributed into 6 sections. Table 3 indicates their positions as a function of the span for each model.

2.2 - Wind Tunnels

The low speed tests were conducted in the S1Ca wind tunnel or in the S2Ch wind tunnel. In both cases, a guided circular test section Eiffel type wind tunnel is used (diameter Ø - 3 m). The maximum speeds are V_o = 40 and 110 m/s respectively and the turbulence rates moderate (t*0.003). These wind tunnels are not pressurized and therefore the range of the Reynolds number (formed with the wing chord) covered is modest: $0.4 \leq Re_c \leq 1.9.10^6$.

High speed studies were conducted in the transonic test section of the S2M wind tunnel [1] where a Mach number of M_o = 1.3 may be reached. All tests could be performed with the same Reynolds Number $Re_c = 2.5.10^6$ due to the pressurization of the wind tunnel. /3

The test section is virtually square (1.75 m x 1.77 m). Only the upper and lower walls are perforated with holes that have a diameter of Ø = 18 mm and are inclined by 60° and the overall perforation rate is 6%.

The model is mounted (figure 2) on the straight solid wall (pilot direction) by means of a turret that assures the formation of an angle of attack. As shown in the photo, a guard plate incorporated with the turret protects the wing from the effects of a parietal boundary layer. The mounting of the MS model in wind tunnels S1Ca and S2Ch is similar.

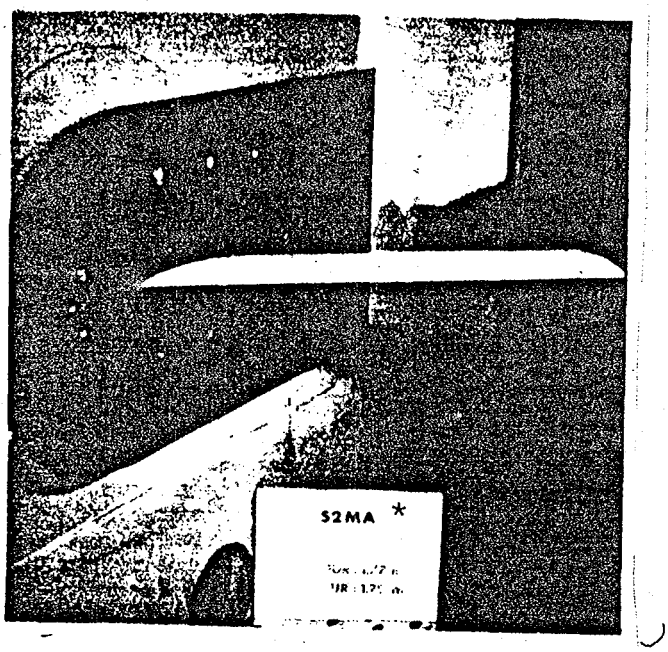

Fig. 2 - Mounting of Model in Transonic Test Section

*S2MA Transonic Test Section
Height: 1.77 m
Width: 1.75 m

2.3 - Testing Techniques

Measurements were made of the overall stresses determined at low and transonic speeds using a 3, 5 or 6 component balance at the wall.

The method of acquiring the static pressure fields on the wing depend on the design itself of each of the two models. It is thus that the pressure measurements made with scanivalves are limited, in the case of an MS model, to two sections per test. Conversely, the MT model permits a full measurement of all static pressures on the wing in a few seconds.

Two techniques of visualizing the parietal stream lines were used. The first, used for the low speed tests, is based on the use of a viscous coating with virtually permanent fluidity which is a mixture of paraffin oil and titanium oxide. The second,

performed everywhere because of its reversibility in a transonic wind tunnel, consists of emitting colored and highly fluid kerosene-based liquids in the model.

Finally, to determine the nature of the boundary layer at low speeds, visualizations were performed of the transition. They are based on technique that sublimates the a thin layer of paradichlorobenzene crystals and naphthalene projected with a gun at the wing's surface.

3 - VARIABLE SWEEP WING AT LOW SPEEDS

In this speed range, three types of flow may be very roughly distinguished. They are found on the top side of this wing as a function of the angle of attack and sweep:

-an unseparated flow at low and moderate angles of attack in the entire range of sweeps used;

-an unseparated and unorganized flow appearing at moderate angles of attack with small sweep or at very large angles of attack with a strong sweep;

-a separated flow, but organized owing to the formation of a horn-shaped eddy with high sweeps ($\Lambda \geq 40°$) and at moderate and strong angles of attack.

The lift curves of figure 3 illustrate this situation quite well and show that the wing behaves at small angles of attack like an infinite wing in an oblique attack.

The linear part of the lift curves corresponds to the first type of flow. The unseparation at the Reynolds number is considered to be sudden for $\Lambda \geq 40°$ the nonlinear part of the lift curves which precede the unseparation is typical of the third type of flow..

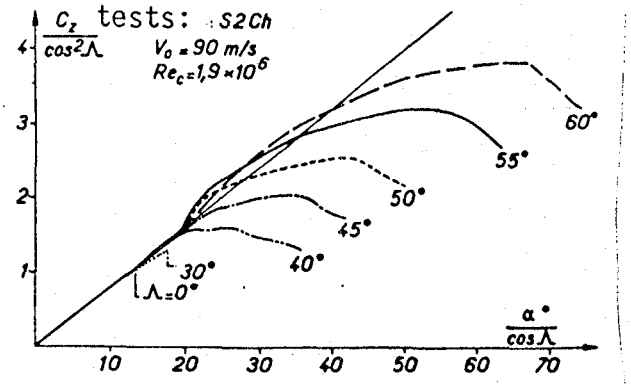

Fig. 3 - Lift and Separation

The flows present prior to separation (types 1 and 3) are analyzed in detail.

3.1 - Flows At Small Angles of Attack

It has already been shown that these flows belong to those of the theory of an infinite wing in an oblique angle of attack. The pressure distributions measured in a median section of the wing justify this assertion. An example /4 is given in figure 4, showing for five sweeps the pressure coefficients kp related to $\cos^2\Lambda$ as a function of the chord $(x_1/c)^{1/2}$* reduced to the same normal angle of attack $\alpha_n = \alpha/\cos\Lambda$. The curves group together fairly well even at the top surface near the leading edge which is the seat of a laminar separation bulb (with turbulent reattachment). At the Reynolds numbers studied this separation bulb caused by the "peaky" nature of the profile determines the position of the transition beginning with very small angles of attack ($\alpha_n \sim 2°$). Consequently the experiment does not reveal on the top side a large effect of the cross flow on the transition position.

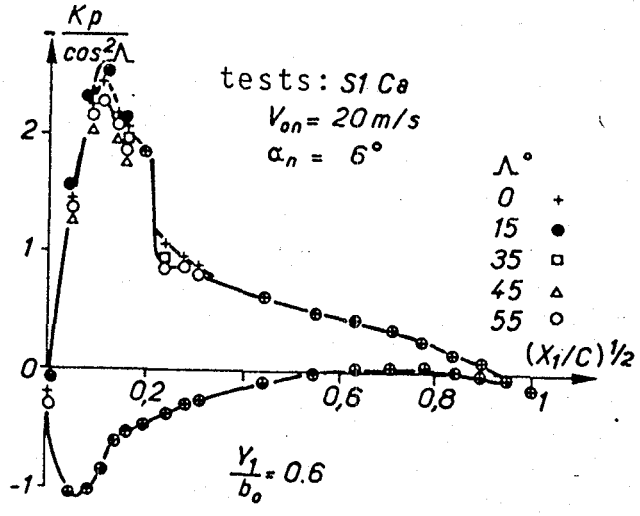

Fig. 4 - Experimental Pressure Distributions

Conversely, this flow appears very distinguishably on the under side, especially when the Reynolds numbers are higher. This is shown in figure 5 which depicts all transition positions on the under side at an angle of attack of $\alpha_n \sim 6°$ as a function of the sweep. The virtually two-dimensional nature of these transition positions should be stressed. The test

*The representation in $(x_1/c^{1/2}$ permits a better representation of the leading edge region.

technique used does not detect potential separations. Therefore the figure gives an indication of the laminar separation point obtained by a calculation made on the assumption of a wing sweep with an infinite span.

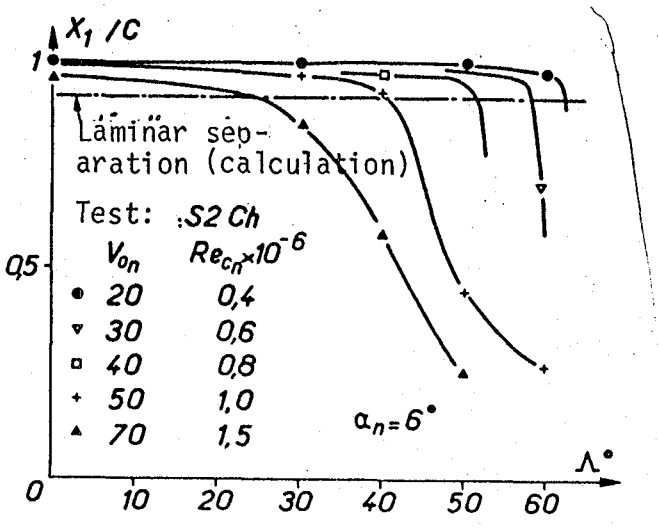

Fig. 5 - Transition Positions on the Under Side.

3.2 - Prediction Methods and Calculation Example

The prediction of unseparated flows around a wing with variable sweep is shown in a conventional manner using a singularities method developed at ONERA over the past few years. To represent the thickness [2] and lift [3] effects, it uses a surface distribution of sources on the wing and a concentrated vortex network located in the medium plane of the wing. The vortex network extends beyond the leading edge of the wing. The equilibrium position of the vortex sheet thus illustrated is determined in advance.

The numerical treatment requires a geometrical discretization of the wing which is depicted by a polyhedron with 460 facets formed by a longitudinal network with 10 sections parallel to the root section, and by a cylindrical network parallel to the leading edge resting upon the edges of a 46 segment polynomial forming the longitudinal profile.

This division of the wing is also used to calculate three-dimensional boundary layers. These are integral methods which were developed according to similar principles and based on identical numerical techniques for laminar and turbulent cases. They are based on the solution of general momentum equations expressed in two directions and on the overall kinetic energy (laminar case)

or continuity [4] equations (turbulent case). It may also be pointed out that these methods were established for a general case of any axis system.

From the practical standpoint, the pressure field calculated using the signularities method is used as the boundary layer calculation datum. The agreement is generally fairly satisfactory when the calculated pressure field is compared with the experiment even for angles of attack close to the separation point as shown in the example of figure 6. The correct prediction of the overspeed peak essentially depends on the discretization of the wing, which in the example given does not observe the truncated form of the wing tip. In this zone the calculated pressure distributions are highly influenced by the shape of the vortex sheet.

Without appropriate testing, it is not easy to check the quality of the boundary layer calculations. However in the example shown a satisfactory prediction is given of the separation of the laminar boundary layer. Then by providing a suitable resetting to account for the bulb passage, the parietal streamlines downstream from the bulb are predicted. This is shown in figure 7 where the variation of the boundary layer β_o of the parietal streamlines is depicted with respect to the streamlines of the potential flow.

3.3 - Vortex Flows At High Sweeps /5

When the sweep reaches or exceeds a value of $\Lambda = 40°$, lift curves are seen with a nonlinear variation as of a an angle of attack of a few degrees. Moreover, the separation angle of attack may be beyond $\alpha = 30°$. This behavior is the effect of the presence of another type of flow on the upper surface of the wing, in a well delimited angle of attack and sweep range. This is a separated flow then the leading edge which is organized by the formation of a horn-shaped vortex generating an appreciable lift gain.

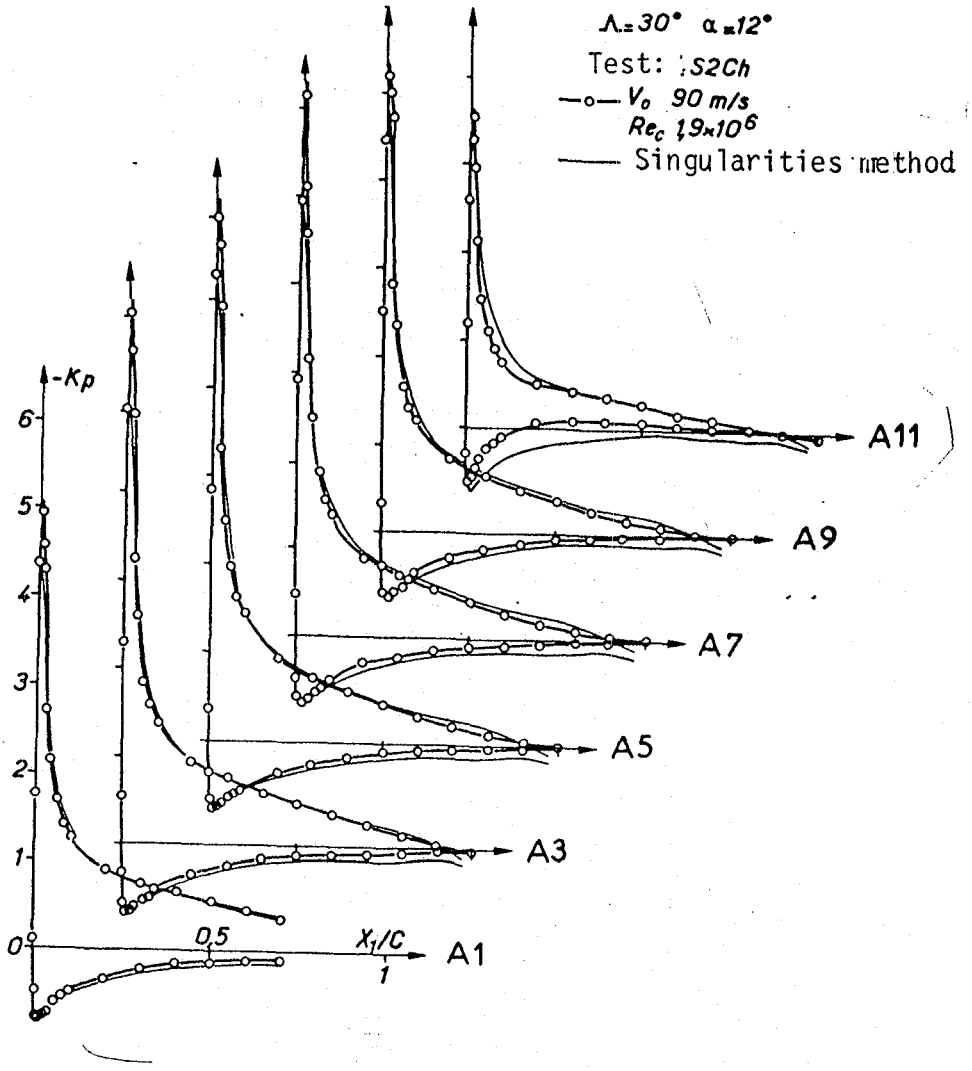

Fig. 6 - Theoretical and Experimental Pressure Distributions

Figure 8 shows, for two Reynolds numbers, the respective ranges for the existence of these vortex flows on the AFV-D wing. Their appearance is determined by a value of a vortex Δcz of 0.22 given the measuring accuracy. The upper limit is defined by the $\alpha cmax$ values of the separation and may therefore be compared with the bursting of the vortex near the apex. Finally, the lateral limit of the range is not known with a great deal of precision because the study of the sweep is conducted in 5° steps. During the passage, one notes the appearance of vortex flows with strong

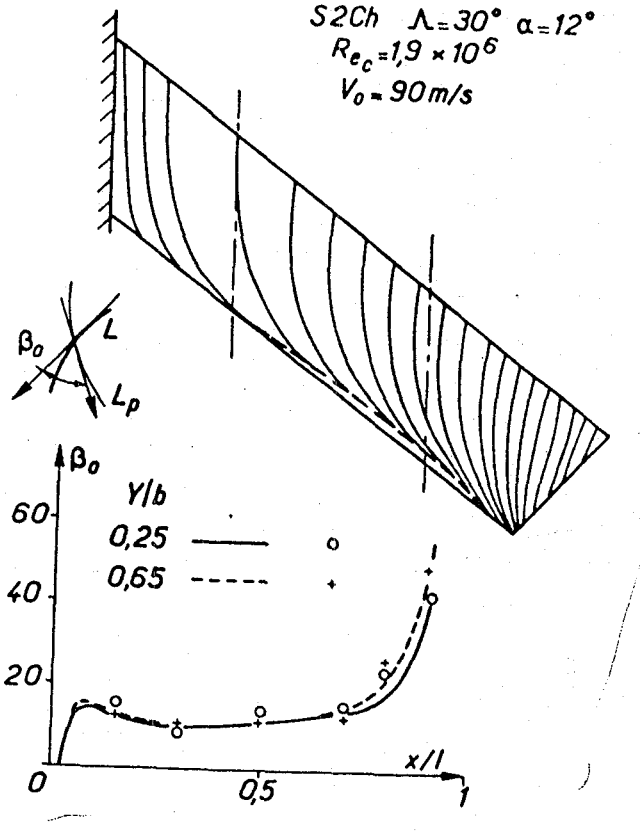

Fig. 7 - Parietal Streamlines. Calculation and Experiment.

sweeps moving toward the angle of attack value observed [15] for slender wings ($\alpha \sim 60°$).

Moreover, these results provide some information on the effect of the Reynolds number. An increase in the Reynolds number by varying the speed V_0 reduces /6 the range for the existence of vortex flows on the AFV-8 wing. Actually, for a given sweep, the angle of attack at which this type of flow appears increases whereas the angle of act of the maximum lift decreases slightly.

This is illustrated even more by the lift curves at Λ = 50° of figure 9. An inspection of the curves relating to the moment of pitch on the same figure show, independently of the Reynolds number, a tendency to dive when a vortex flow appears and is followed by a long nose-up. This obviously shows the variation of the center of thrust under the effect of the horn vortex.

The repercussion of the appearance of this vortex on the upper surface flow is shown in figures 10 and 11. These depict, respectively, the pressure fields and the parietal visualizations obtained by the coating in the case Λ = 50° and α = 12° for two different Reynolds numbers. At the highest Reynolds number, the pressure distributions indicate an essentially unseparated flow with a strong overspeed peak at the leading edge. We see (figure 10) that the signularities method mentioned above predicts this type flow fairly accurately. Conversely, at a lower Reynolds number

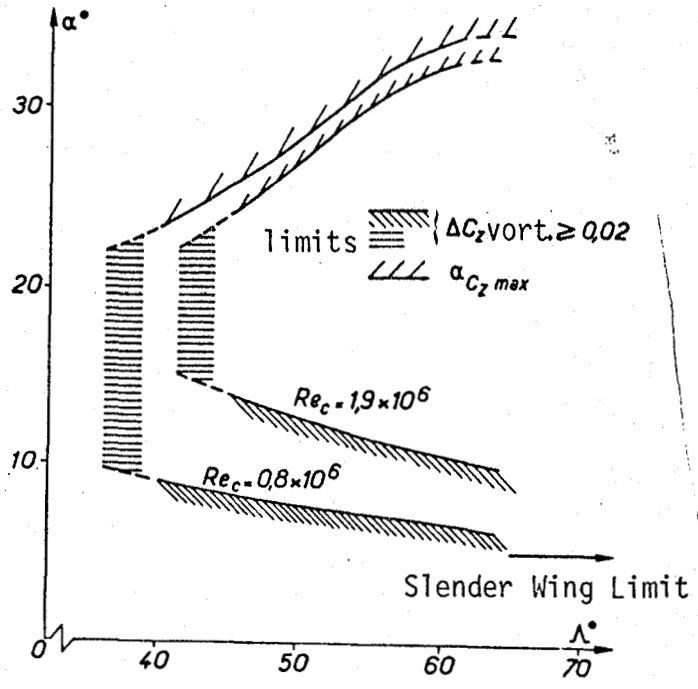

Fig. 8 - Range for the Existence of Vortex Flows.

a more general separation occurred. It organizes itself perfectly to form a horn vortex whose path passes through the wing and appears on the pressure distributions and on the parietal visualizations.

3.4 - Theoretical Approach and Comparison with Experiments

Owing to the increaseing interest given to vortex type flows, special efforts have been made to predict them. A three-dimensional method of calculating vortex sheets in a perfect fluid is being developed at ONERA [5], [6], [7].

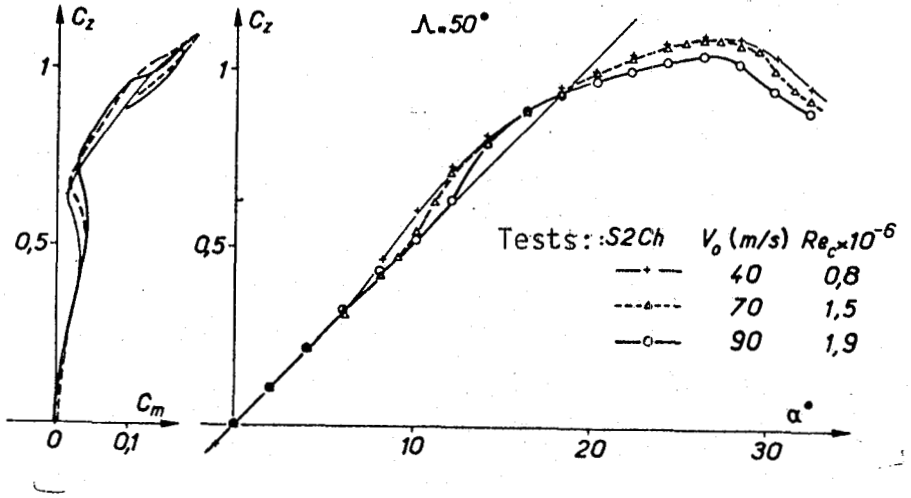

Fig. 9 - Lift and Moment of Pitch. Effect of Reynolds Number.

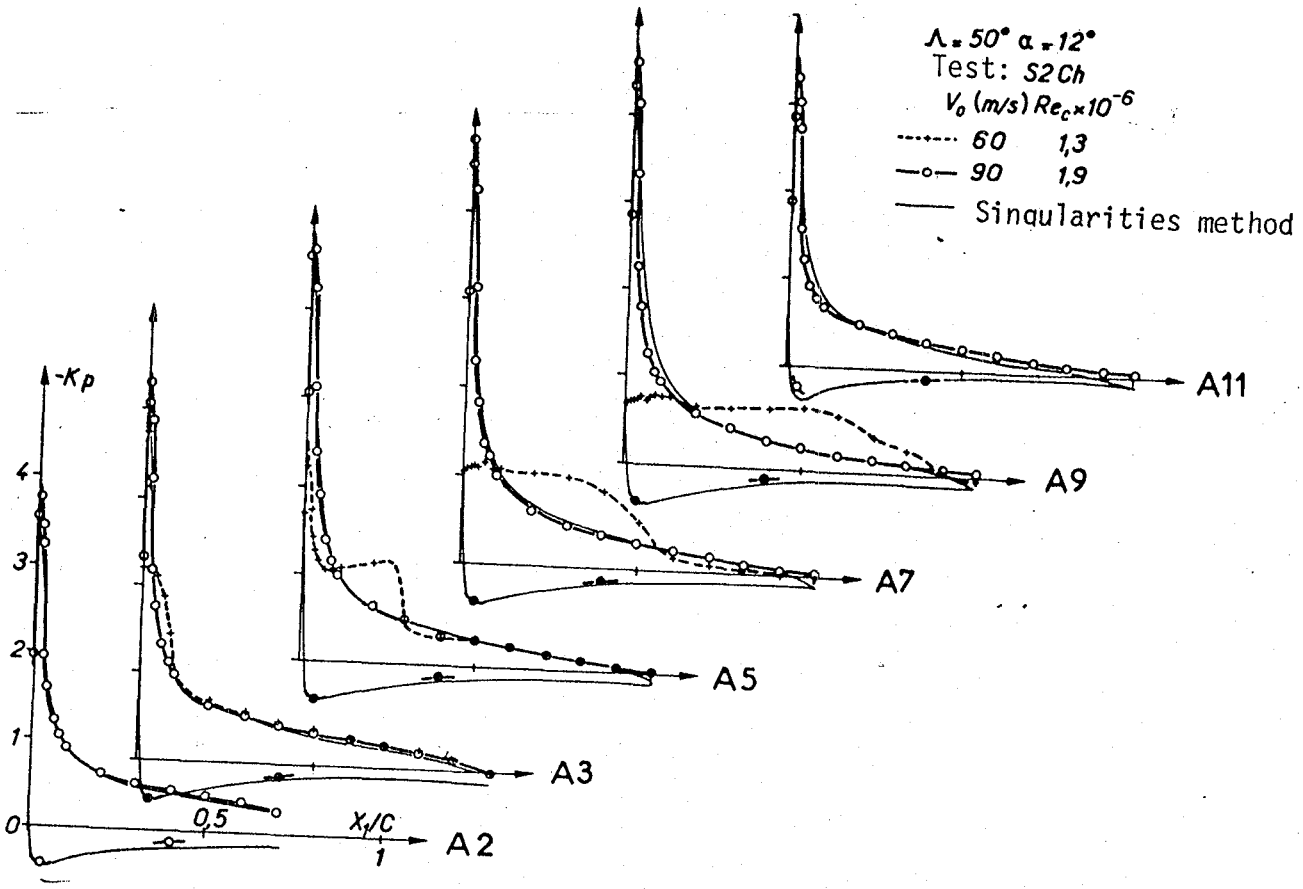

Figure 10 - Theoretical and Experimental Pressure Distributions.

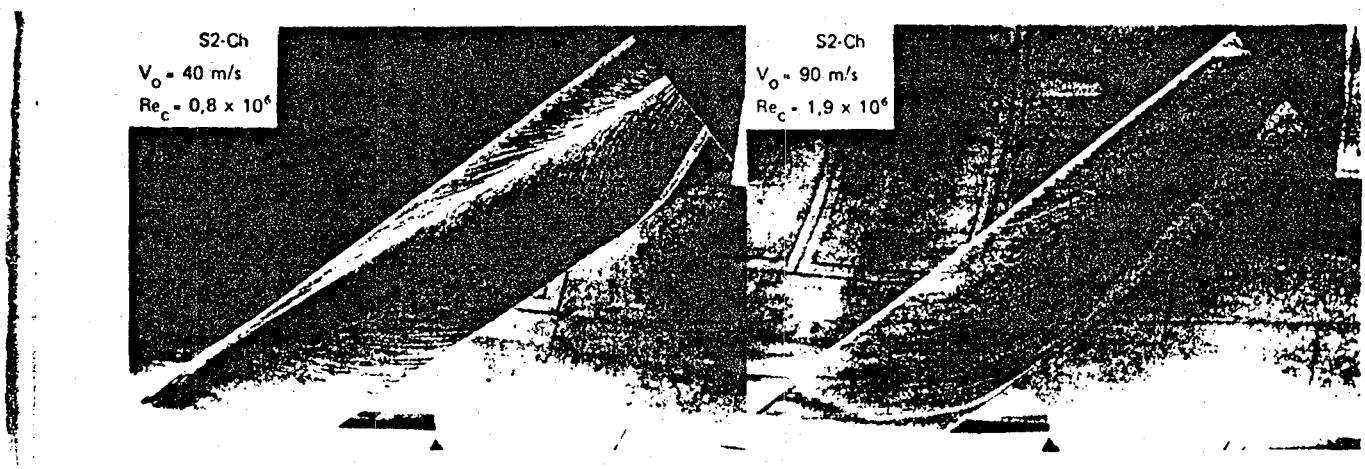

Figure 11 - Visualizations of Parietal Streamlines.
Λ=50° α=12°

This method, based on the application of Lagrange's variables to an integro-differential system discretisized using specific singularities makes it possible to monitor the vortex particles emitted at the trailing edge at the tip and at the leading edge of the wing. Currently, it is applied only to infinitely thin wings.

In order continue evaluating this method, an application was made to a wing with variable sweep. This is the case of $\Lambda = 60°$ and $\alpha = 24°$ selected owing to the stability of the horn vortex observed experimentally in both a wind tunnel and in a hydrodynamic tunnel where spatial visualizations were made. These were remarkable in terms of the vortex flows. In order to calculate, the wing was discretisized by 75 doublets facets each having a control point to satisfy the slip condition. Furthermore, 30 points were defined on the /8
wing contour (15 of which were located on the leading edge) where vortex particles are emitted.

Figure 12 shows the emission lines calculated at instant $\tau = 1,2$ ($\tau = 1$ corresponds to the time it takes for a particle moving at the reference speed V_0 to travel the distance of the chord ℓ) and compared with a visualization made in a hydrodynamic tunnel for a very close angle of attack. A differences diagram, accurate at $0(\Delta\tau^2)$ was used in this calculation. The emission lines issuing from the leading edge reveal the tendency for a horn vortex sheet to form, observed on the visualization. However numerical problems due among others to an excessive rapprochment of the vortex elements currently prevent a steady solution ($\tau > \infty$) as shown in figure 13.

This figure shows, as a function of time τ, the variation of the normal calculated force C_N. With the result of the calculation case already discussed are shown two other results for the test calculation made at $\alpha = 12°$ and $24°$ in which the emission of the vortex particles is limited to the trailing edge and to the tip. In these relatively academic cases (academic, because they are unsuitable for predicting separated flows), the computation method

Testing in a Hydrodynamic Tunnel

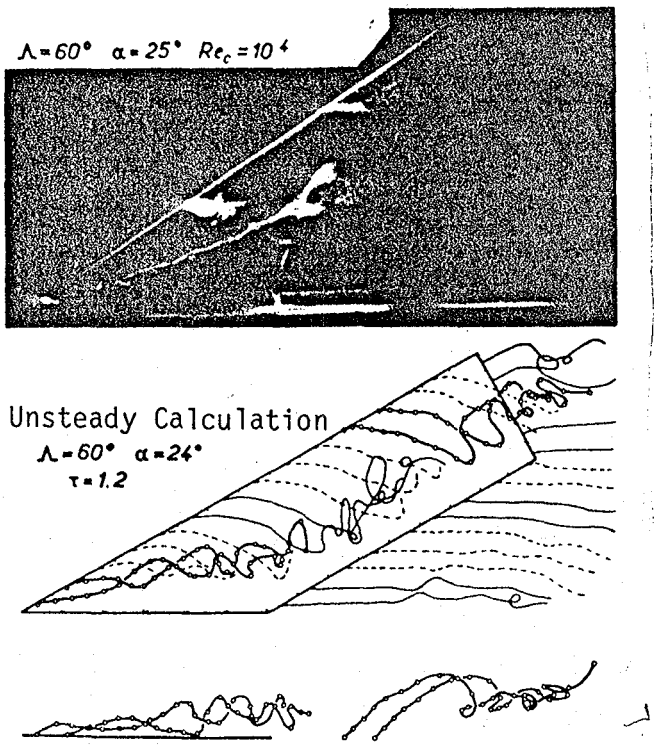

Fig. 12 - Emission Lines - Analogy Between Observation in Hydrodynamic Tunnel and Unsteady Calculation.

gives results that tend to move toward a limit without any problem, which is the steady solution. In the case of a small angle of attack $\alpha = 12°$ we then obtain a value of the normal force C_N which is fairly close to the experimental value.

At this angle of attack, the absence of a considerable vortex effect (figure 14) explains this result. The latter figures illustrates that the difference between the theoretical results and experimental results, for both cases, corresponds to a small vortex lift for $\alpha = 12°$ and large for $\alpha = 24°$.

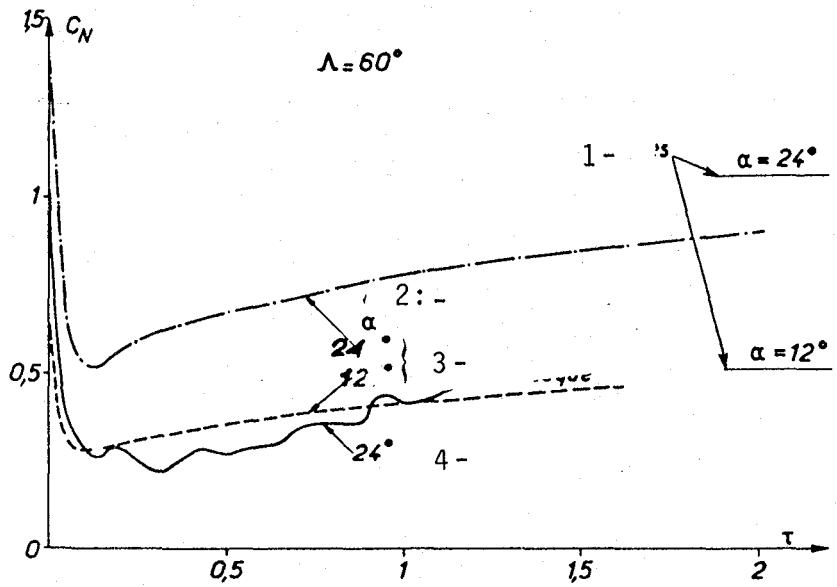

Fig. 13 - Variation as a Function of Time of the Normal Theoretical Force.

Key: 1-Steady experimental values; 2-Unsteady calculations; 3-Without separation at leading edge; 4-With separation at leading edge.

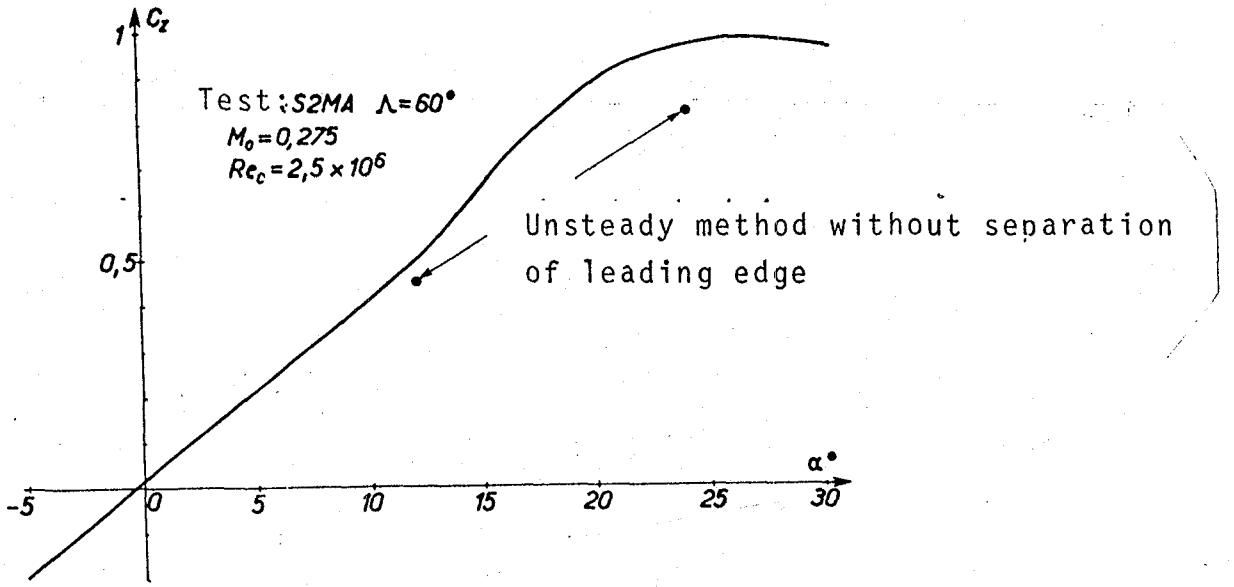

Fig. 14 - Lift. Calculation and Experiment

4 - VARIABLE SWEEP WING IN A TRANSONIC FLOW

It is not possible within the scope of this report to fully describe the often highly complex flows which were revealed as a function of the sweep, of the Mach number and of the angle of attack in the S2MA wind tunnel.

A group of these results however was selected [8] by an AGARD-FDP task force formed to collect very complete and reliable experimental data and to compare them with the computation results. In this regard, it should be pointed out that the obstruction rate of the model in the test section is slow and does not exceed 0.5%. Accordingly, no correction was made of the experimental results.

4.1 - Sweep Effect in a Supercritical Flow

To give an idea of the different flow forms observed, an analysis of the sweep effect at $M_0 = 0.84$ is proposed. Figure 15 shows the static pressure distributions at $\alpha = 4°$ into two wing sections for sweeps $\Lambda = 0.30$ and 40°. In all cases the fairly sudden recompressions indicate the shock wave positions. At $\Lambda = 0$

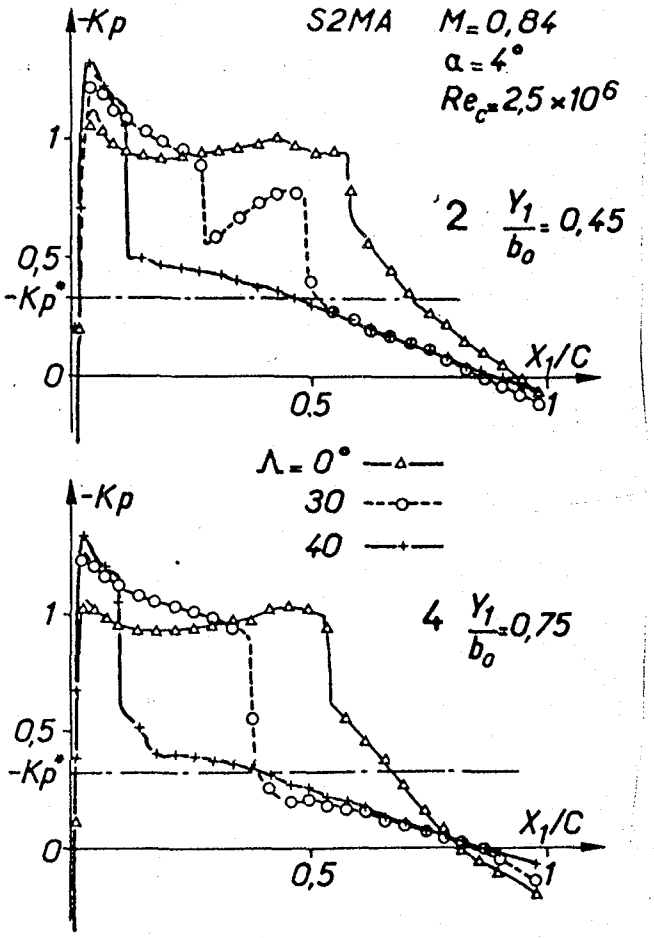

Fig. 15 - Experimental Pressure Distributions

the supersonic zone reaches beyond the half chord. The flow remains virtually two-dimensional despite a turbulent separation caused by the shock and revealed by parietal visualizations. At $\Lambda = 30°$, we see a double recompression toward the root in section 2. The flow remains supersonic behind the first one. Toward the outside (section 4), a single shock exists and the parietal shocks no longer reveal the separation. At $\Lambda = 40°$ the shock appears near the leading edge and the flow preserves a virtually two-dimensional nature.

An examination of all sections leads to the representation of the shocks in figure 16 revealing for example for $\Lambda = 30°$ a lambda form of the shock system which reaches, at $\alpha \neq 40°$ only at $\alpha = 6°$.

At this angle of attack, a general withdrawal of the shock waves is noted. The intensity has increased and with it the tendency for separations. /10

When, still at sweep $\Lambda = 40°$, the angle of attack reaches a value of $\alpha = 8°$ the shock system at the root persists on seeing the pressure distributions, figure 17, but toward the root, a separated and unorganized flow region is observed.

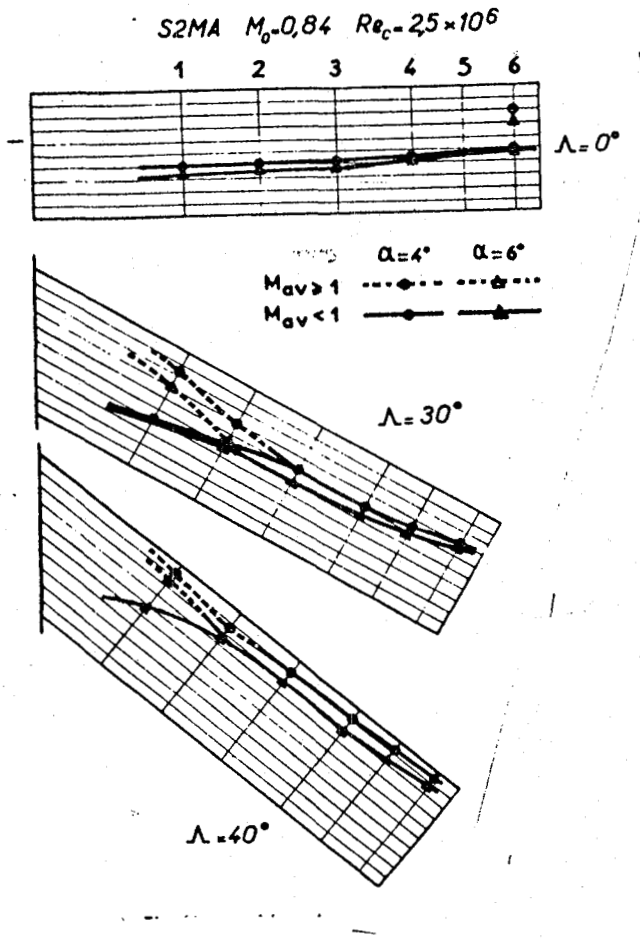

Fig. 16 - Shock Wave Positions

Figure 18 shows that such an organization of the separation stants forming by increasing the sweep to $\Lambda = 60°$ at the same angle of attack.

We finally reach a vortex flow for angle of attack $\alpha = 10°$. This flow is well established this time (figure 19) and is characterized by high values of the pressure coefficient kP_{min}, as the minimum pressure point indicates the axis of the horn vortex, that is now formed, in a first approximation.

4.2 - Calculation Methods and Discussion of Results

On a world-wide scale, considerable effort has been made

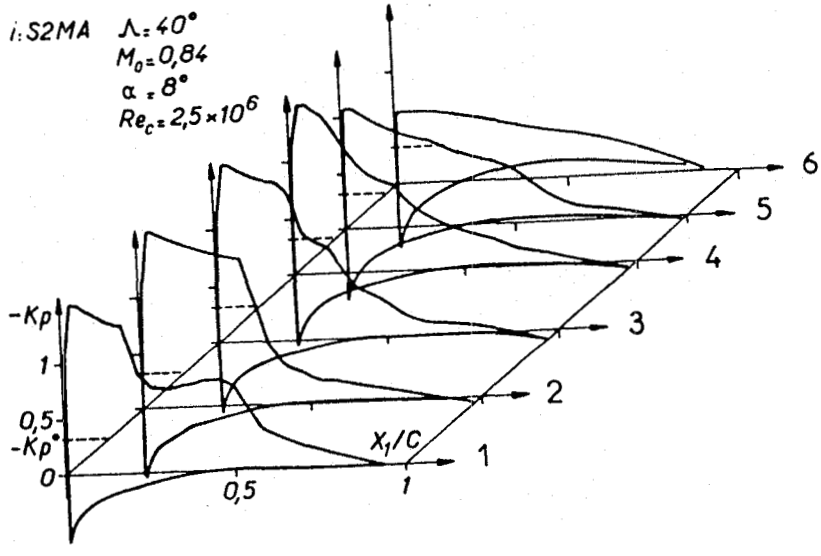

Fig. 17 - Separation Variation - Sweep Effect (1).

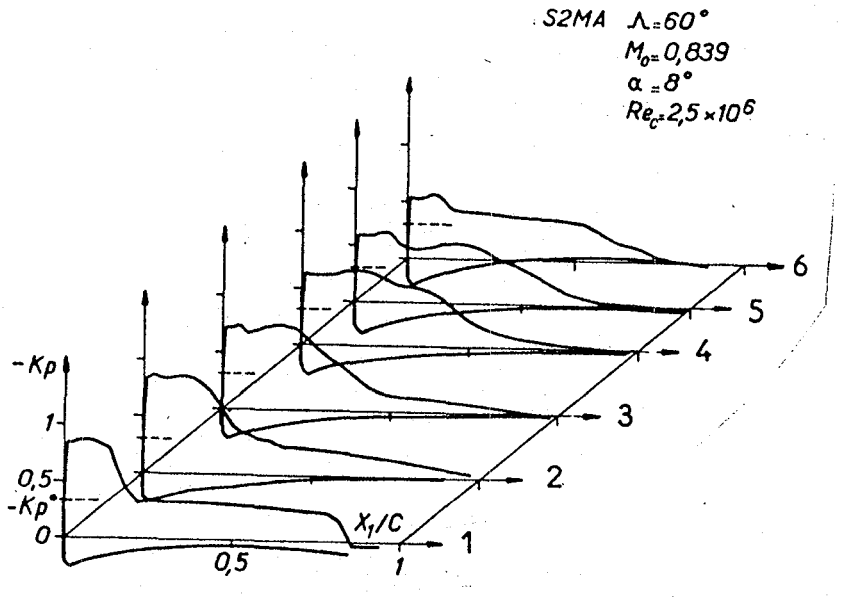

Fig. 18 - Separation Variations. Sweep Effect (2)

over the past few years in developing methods of calculating three-dimensional transonic flows about wings. At ONERA relaxation methods have been chosen for solving the complete equation of the potential [9], [10].

First, the equation was used in a quasi-linear form and discreticized using a mixed scheme [11]. More recently, the equation was expressed in a conservative form, including the artificial viscosity in the expression [12]. The discretization shemes used are centered and the resolution method is associated with an approximated factorization method. Moreover, by virtue of a cooperative agreement with the DORNIER Company, we have a third method of relaxation [13] [14], based on an essentially more restrictive approximation, namely the small disturbances equation solved using a mixed scheme.

The application of all these methods to a variable sweep wing which is represented with one tip parallel to the root calls for a few clarifications about the expansion of the calculations.

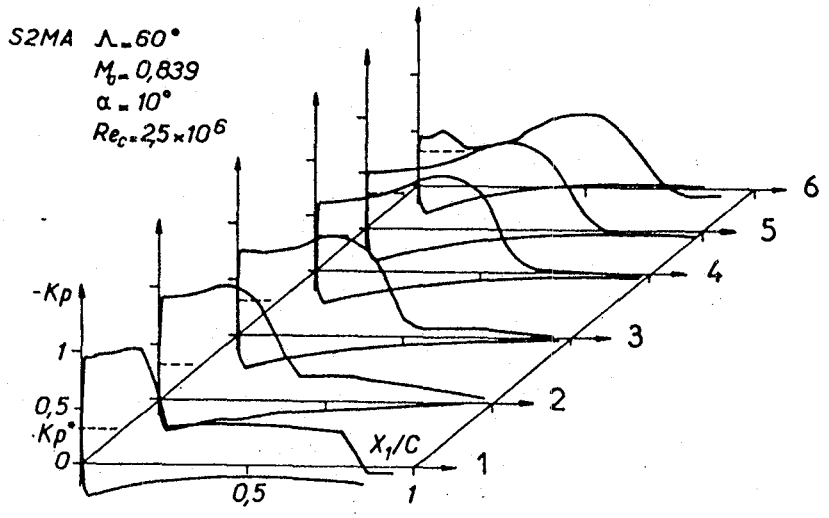

Fig. 19 - Organized Separation. Established Vortex Flow

When a full potential equation is solved, the calculation is approached using a conservative method in a rough meshing (about 16,000 points) with a number N of iterations that varies with the treated case ($500 \leq N \leq 800$). The potential is then interpolated with the nodes of a fine grid (about 65,000 points) upon which the calculation is converged by $40 \leq N \leq 80$ more iterations. When a conservative method is used, the fine meshing counts only 96 x 32 x 16 = 49 152 points because of the limitations of the main memory of the computer used. This procedure makes it possible to economize a certain number of fine meshing cycles representing the largest portion of the calculation expenditure. The convergence is defined based on an examination of part of the calculation residue and on the development of the solution.

In solving the disturbance potential equation, the calculation is done in a rectangular meshing associated with the model which does not undergo any changes during the computation. Accordingly, the meshing is adapted to each sweep angle, but does not exceed 55,000 points for the same reasons given above. In this case as well a fairly high number of iterations may be required ($400 \leq N \leq$) in order to obtain a converged solution.

A few typical results of computations performed by these different methods will be described below. They will be compared with the experimental results for which it was verified that the boundary layers on the upper surface and on the under surface of the wing remain laminar until the recompressions begin. When the gradient of the recompression is strong enough, the formation of small laminar separation bulbs is observed. This phenomenon appears more specifically when the flow is subcritical or even at the level of the shock wave, still on the upper surface, in the case of a supercritical flow.

The first example pertains to a wing placed in a sweep $\Lambda = 40°$, with a Mach number $M_o = 0.78$ and at an angle of attack $\alpha = 2°$. One exception is the supersonic zone limited to the region of the leading edge where the overspeed point is located. The flow is almost subcritical and without shock. Figure 20 illustrates for section 3 a comparison between the experiment and the results of the calculaton after interpolation. In this case where the three-dimensional effects remain small, a very good agreement may be observed between the experimental and theoretical pressure distributions relative to the solution of the full potential equation. The solution using the small disturbances method is also very correct except right near the leading edge. This is a classical error of methods using small disturbances equations.

The following result, shown in figure 21 for the same section, pertains to a clearly supercritical configuration with the parameters $\Lambda = 0°$, $M_o = 0.84$ and $\alpha = 0°$. It is particularly the prediction of the shock and its extension to the various calculations which calls for a comment. Comparing the results obtained from the full equation using conservative and unconservative schemes /12 there is not much difference in the position of the calculated shocks. The expansion observed with the conservative shceme is ude to a fairly undense meshing in the median part of the profile. However a pressure jump is fairly well predicted by this method,

and by the small disturbances method, also made conservative using a shock operator. The experiment indicates a slightly more rearward shock position than the set of calculations.

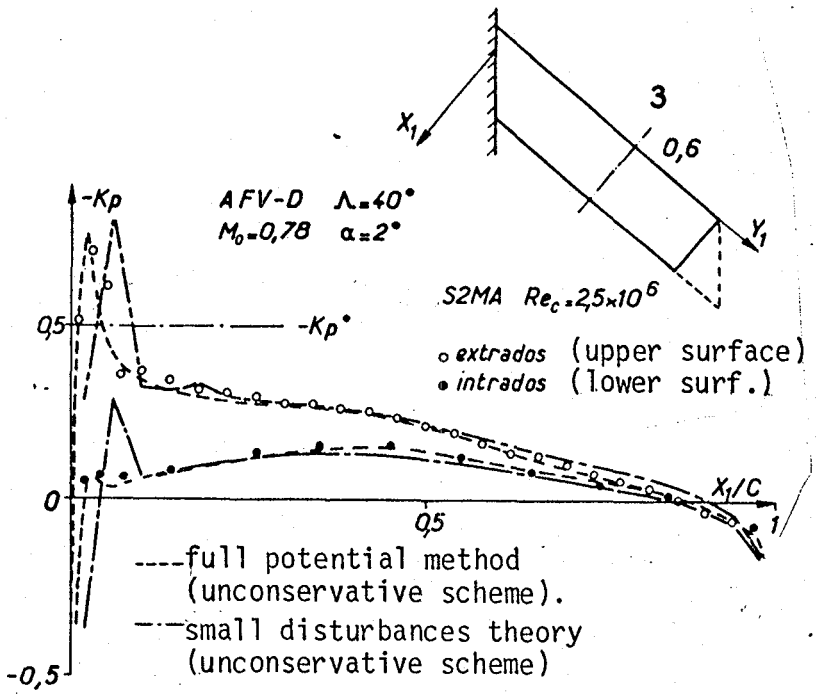

Fig. 20 - Theoretical and Experimental Pressure Distribution. Subcritical Case.

This is also true in in the following example where the wing is placed with a sweep $\Lambda = 30°$, still at Mach $M_0 = -.84$, but at ang angle of attack $\alpha = 40°$. Figures 22 and 23 clearly show the progress due to the conservative scheme although without perfect agreement with the experiment. This case is characterized by a system with two shocks appearing on the supper surface toward the root, whereas toward the tip only a single shock remains.

This time with the conservative scheme a better agreement is obtained with the experiment than with an unconservative scheme which predicts a much more forward shock position. It is noticed however that the pressure coefficient level kp in the supersonic zone remains inadequate relative to the measurments. Despite the appearances (figure 23) the calculation predicts fairly well, toward the root, the reacceleration of the flow downstream from the first shock, but it does not reach the extension observed experimentally.

If no major problem appeared while performing the calculations just shown, an attempt was made to process a supercritical case with a stronger sweep and this did not give a satisfactory solution. This case corresponds to a wing configuration with a sweep $\Lambda = 40°$

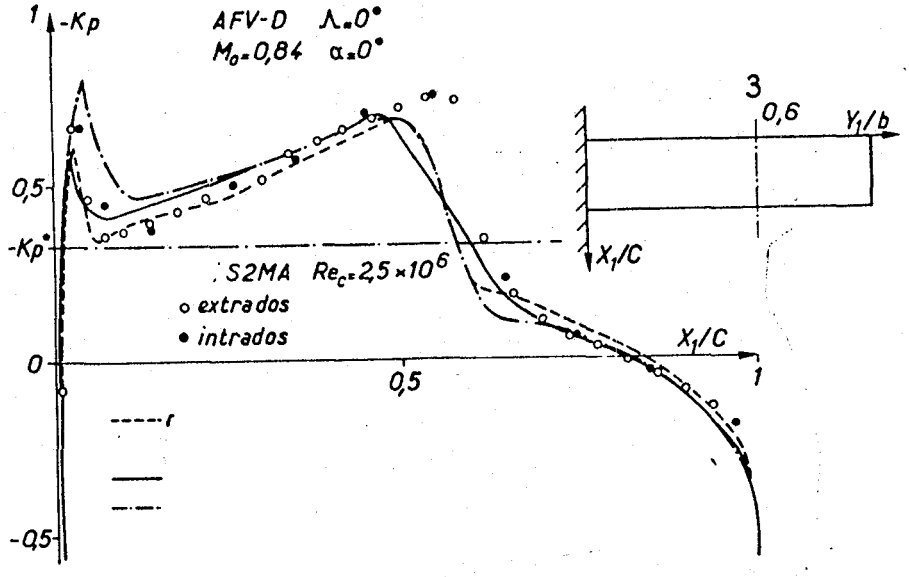

Fig 21 - Theoretical and Experimental Pressure Distributions. Supercritical Case (1).

----full potential method (unconservative scheme)

____full potential method (conservative scheme)

-·-·- small disturbances theory.

With a Mach number M_0 = 0.92 and an angle of attack α = 1.53°. A comparison between the current calculation results and the experiment is shown in figure 24. Compared to the experimental pressure /13 distribution, what is particularly noticeable is the absence of a satisfactory prediction of the rear shock using the method solving the full potential equation and to a lesser degree, by that of the small disturbances theory.

5 - CONCLUSIONS /14

Tests conducted at ONERA in the various sub and transonic wind tunnels on models of a rectangular wing whose sweep can be varied up to Λ = 60° form the experimental base for studying three-dimensional flow. The results make it possible to analyze the flow organization as a function of the sweep, the angle of

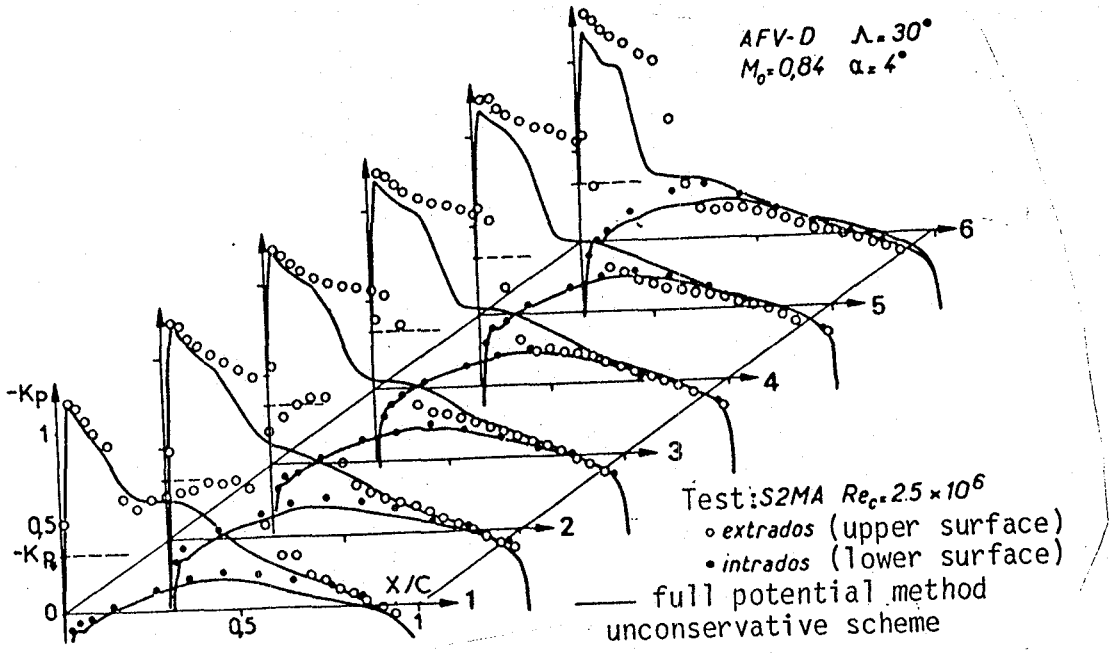

Fig. 22 - Theoretical and Experimental Pressure Distributions. Supercritical Case (2a).

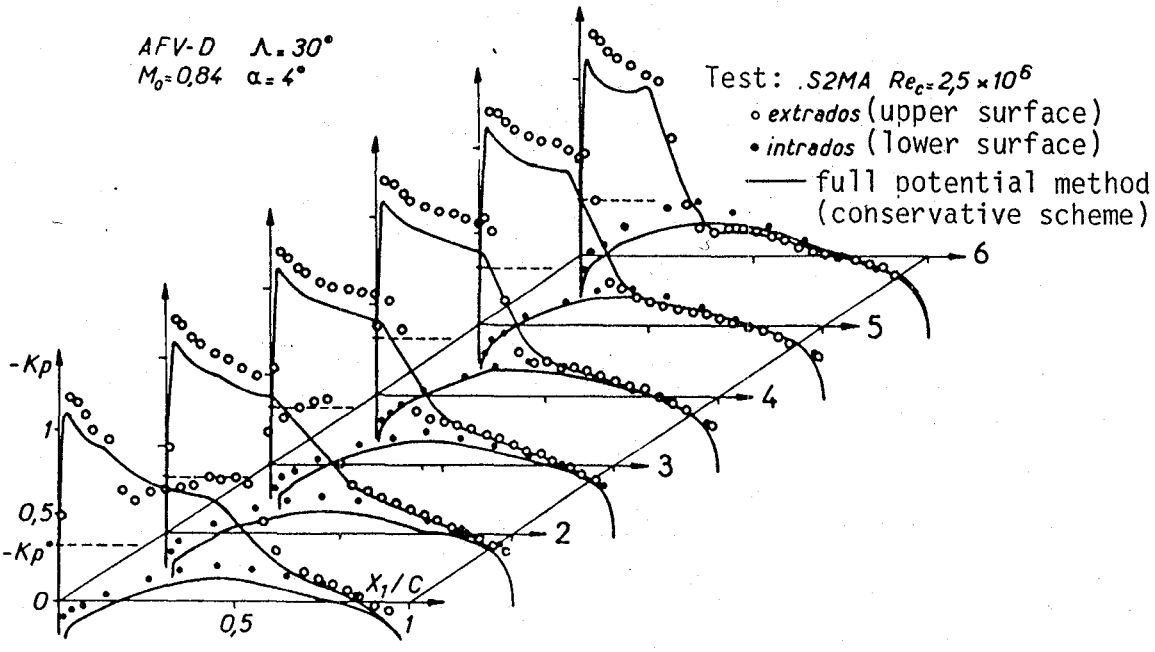

Fig. 23 - Theoretical and Experimental Pressure Distributions. Supercritical Case (2b).

attack and the Mach number. They have also proven to be very useful for developing computer methods.

At low speeds, and for unseparated flows, the predictions using conventional singularities methods are fairly satisfactory.

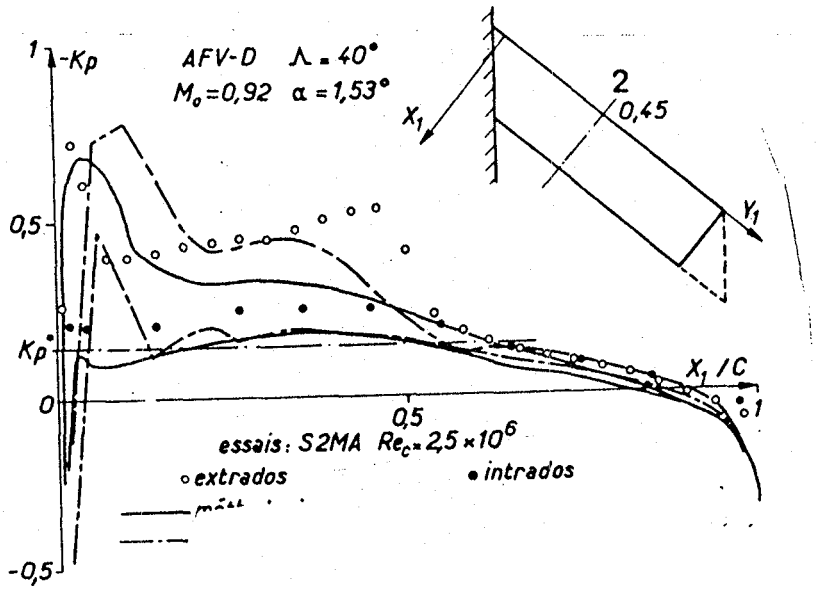

Fig. 24 - Theoretical and Experimental Pressure Distributions. Supercritical Case (3).

_____full potential method (conservative scheme)

___ . ___ small disturbances theory.

Conversely, focus should be given to the development of computational methods to predict separated flows which, at high sweeps, organize themselves by forming a horn vortex. The unsteady method shown here seems to be promising in this respect.

In the transonic regime, considerable progress has been made over the past few years by developing relaxation methods for solving disturbance potential and full potential equations. The exact limits of their use are not yet known.

REFERENCES

1. PIERRE M. - FASSO G.

   The Aerothermodynamic Test Center of Modane-Avrieux
   ONERA - Technical Memorandum No. 166E (1972).

2. HESS J. - SMITH A.

   Calculation of Non-Lifting Potential Flow About Arbitrary Three-Dimensional Bodies.
   Douglas Aircraft Company. Report No. E.S. 40622 (1962).

3. RUBBERT P.E. and al.
   A general Method for Determining the Aerodynamic Characteristics of Fan-In-Wing Configurations.
   Volume I: Theory and Application
   The Boeing Company - Document AD 667 980.

4. COUSTEIX J.

   Theoretical Analysis and Prediction Methods of Three-Dimensional Boundary Layer.
   ONERA Publication No. 157 (1974).

5. REHBACK C.

   Numerical Calculation of Three-Dimensional Unsteady Flows With Vortex Sheets.
   Aerospatiale Study No. 1977-5, p. 289-298, (1977).

6. REHBACH C.

   Numerical Calculations of Three-Dimensional Unsteady Flows With Vortex Sheets.
   AIAA Paper No. 78-111 (1978).

7. REHBACH C.

   Unsteady Calculation of Vortex Sheets Emitted by Highly Inclined Lifting Airfoils.
   "High Angle of Attack Aerodynamics"
   AGARD-CP (to be published).

8. MANIE F. - RAYNAL J.C.

   Transonic Measurements on the ONERA AFV-D Variable Sweep Wing in the ONERA S3MA Wing Tunnel.
   AGARD-AR (To be Published).

9. CATTOT J.J. - COULOMBEIX C. - TOME C.

   Transonic Flow Calculations About Wings.
   Aerospatiale Study No. 1978-4 (to be published).

10. CHATTOT J. - COULOMBEIX C. - MANIE F - SCHMITT V.

Transonic Flow Calculations About Wings.
Report presented at Symposium on "Transonic Configurations" of DGLR at Bad Harzburg (FRG), June 1978.

11. MURMAN E.M. - COLE J.D.

Calculation of Plane Steady Transonic Flows.
AIAA Journal, Vol. 9, No. 1, p. 114-121 (1971).

12. JAMESON A.

Transonic Flow Calculations.
AGARD-LS 87 (1976).

13. SCHMIDT W. - VANINO R.

The Analysis of Arbitrary Wingbody Combinations in Transonic Flow Using a Relaxation Method.
Symposium Transsonicum II, Gottingen (1975).

14. SCHMIDT W.

Progress in Transonic Flow Computations - Analysis and Design Methods for Three-Dimensional ,lows.
AGARD-LS 87 (1976).

15. REBUFFET P.

Experimental Aerodynamics
Volume 2 - Dunod, Paris, (1966).